

Numerical study of steel box girder bridge diaphragms

Shervin Maleki*, Pantea Mohammadinia^a and Abouzar Dolati^b

Department of Civil Engineering, Sharif University of Technology, Tehran, Iran

(Received January 6, 2016, Revised October 4, 2016, Accepted October 5, 2016)

Abstract. Steel box girders have two webs and two flanges on top that are usually connected with shear connectors to the concrete deck and are also known as tub girders. The end diaphragms of such bridges comprise of a stiffened steel plate welded to the inside of the girder at each end. The diaphragms play a major role in transferring vertical and lateral loads to the bearings and substructure. A review of literature shows that the cyclic behavior of diaphragms under earthquake loading has not been studied previously. This paper uses a nonlinear finite element model to study the behavior of the end diaphragms under gravity and seismic loads. Different bearing device and stiffener configurations have been considered. Affected areas of the diaphragm are distinguished.

Keywords: steel bridge; tub girder; end diaphragm; seismic; cyclic behavior

1. Introduction

The extensive application of steel box girders in the construction of long span bridges has led researchers to better understand their performance under gravity and lateral loads. Albeit the broad use of these girders, their components behavior has not been scrutinized by researchers. The end diaphragms of steel box girders are one of these components that play a major role in transferring vertical and lateral loads to the bearings and substructure. Bridge performances during previous earthquakes show that steel end diaphragms could be affected by earthquake loads. In some cases steel end diaphragms undergo significant damages (Yen *et al.* 2011, Schexnayder *et al.* 2014).

The first effort in understanding the steel diaphragm behavior was made in 1970 when the failure of load bearing diaphragm triggered the collapse of the Milford Haven Bridge in England during the course of its erection and consequently the Merrison committee was formed and conducted research about the large stiffened diaphragms (Einarson *et al.* 1982). During 1971 to 1972, the first experimental study on diaphragms has been carried out with testing the six large-scale stiffened rectangular load bearing diaphragms by Dowling *et al.* (Dean and Dowling 1973, Dean 1975). The test was conducted in the elastic range and finally to collapse of all diaphragms. Following the first efforts, Irwin and Loe (1978) performed three experimental analyses on trapezoidal box diaphragms. Furthermore Crisfield and Pulthi (1977) verified the elasto-plastic

*Corresponding author, Professor, E-mail: smaleki@sharif.edu

^aM.Sc. Graduate, E-mail: pantea_mohammadinia@yahoo.com

^bPh.D. Student, E-mail: dolati_abouzar@mehr.sharif.ir

elasto-plastic buckling theory for stiffened diaphragms considering interaction of the other components. The research was done based on simple boundary conditions which were not complying with the reality. In order to achieve the simplified rules, Einarrson *et al.* (1982) examined two slender diaphragms without any stiffeners under vertical load. The analysis resulted in an equivalent failure vertical load which was helpful for better understanding the failure mechanism. In 1995, Megson and Hallak (1995a) conducted an experimental test along with numerical modeling using the finite element method (FEM) and compared results. The test specimen was a 1.2 m long stiffened rectangular box girder with a plate diaphragm in the middle. Later, they studied the effective parameters such as height to thickness ratio, height to width ratio and the location of stiffeners and found the equivalent vertical failure load for each configuration (Megson and Hallak 1995b, c, d). More recently, several studies are conducted by Memberg *et al.* (2002), Helwig *et al.* (2007) and Helwig and Yura (2012) in order to provide design guidelines for the diaphragms of box girder bridges. The studies have helpful suggestions for estimating the size of components in order to have suitable stiffness and strength under vertical loads in straight and horizontally curved bridges. Also in relation to the topic, Chusilp *et al.* (2002) did experimental and analytical investigation on box girders under cyclic shear load. On a related note, Park *et al.* (2005) studied the effect of intermediate diaphragm spacing on horizontally curved box girders. Kim and Yoo (2006, 2009) studied the brace forces and bending effects in internal cross-frames of tub girders. Moreover, several researches on modeling procedure and design of box girders have been conducted. Kim and Williamson (2014) elaborated on finite element modeling of twin tub girders. Nie and Zhu (2014) developed a beam truss model for box girders. Samarasinghe *et al.* (2012) studied the redundancy of twin tub girders. Zsarnóczay *et al.* (2014) studied the seismic behavior of conventional girders including the steel box girder. Kaveh *et al.* (2014) proposed an integrated based optimization procedure for box girder design which led to about 15% of saving material. Kargarmokhar *et al.* (2015) investigated the effects of Reynolds number on aerodynamic characteristics of twin deck bridges with the aim of girder design improvement.

Despite the above researches on the effects of vertical loading on diaphragms of box girders, there are many parameters involved that add to the complexity of behavior. Parameters such as, the shape of the box girder, number and location of stiffeners and their welds, number, location and type of the bearing devices underneath, and the geometry of the diaphragm and its boundary conditions make a unique solution almost impossible. Adding the seismic lateral loading makes the problem even more tedious.

As mentioned above, almost all of the researches have been conducted under static vertical loads and seismic response has not been attended. As a result, there is no distinct procedure for designing new diaphragms and choosing its configurations under combined vertical and seismic loading in the design codes. This research is an attempt to fill this gap by numerically investigating the behavior of end diaphragms of a U shaped steel box girder (also known as tub girder) under both vertical and lateral cyclic seismic loads. Moreover, suggestions for the design of stiffened diaphragms under gravity and seismic loads are given.

2. Analytical models

In order to provide a comprehensive numerical study on steel diaphragm behavior, an existing bridge is selected as a reference model. The Khan steel tub girder bridge located in Marvdasht highway of Iran is chosen as a case study. The bridge was designed based on the allowable stress

design method of AASHTO (2002). Fig. 1 shows the configuration of the case study bridge with its steel diaphragm seating on top of a rectangular elastomeric bearing pad. The bridge has two simply supported spans of 38 m each. The steel tub section connects to a 20 cm concrete slab on top via channel shear connectors to benefit from composite action. The bridge supports are designed to carry 40 MN of vertical reaction due to dead plus live loads at each end. The steel end diaphragm of this bridge is used as a reference model and a parametric study is conducted by altering the important components of it. The components of a steel diaphragm are illustrated in Fig. 2.

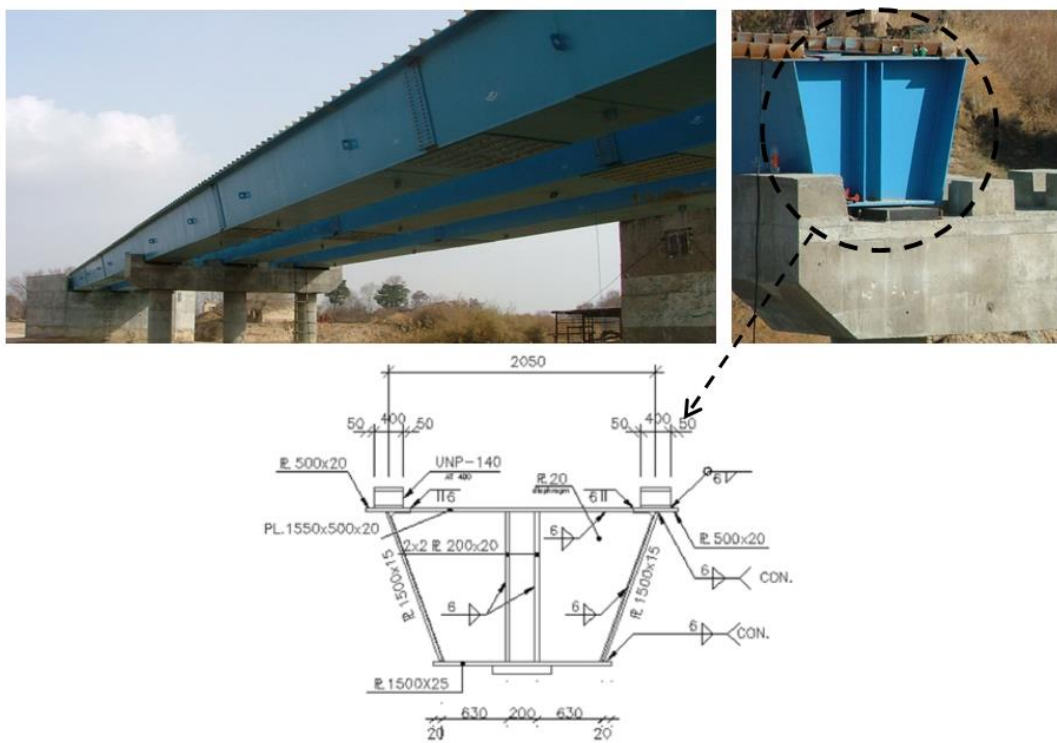


Fig. 1 The case study bridge with its steel diaphragm detail

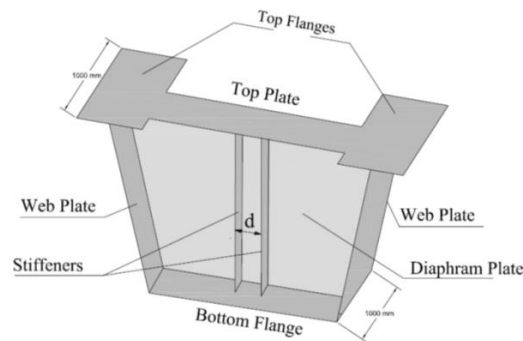


Fig. 2 Components of a box girder and its diaphragm

Table 1 Variable parameters of FE models

Model	Total area of bearing supports cm ²	Bearing dimension length×width cm×cm	No. of bearing pads	No. of vertical stiffeners	distance between stiffeners=d cm
Model 1-A	900	30×30	1	2	20
Model 1-B	900	30×30	1	2	30
Model 2-A	2500	50×50	1	2	20
Model 2-B	2500	50×50	1	2	50
Model 2-C	2640	88×30	1	2	50
Model 2-D	2640	88×30	1	2	88
Model 2-E	2640	88×30	1	3	44-44
Model 2-F	2600	65×40	1	2	65
Model 3-A	2700	27×50	2	2	37
Model 3-B	2700	27×50	2	4	27-20-27
Model 3-C	2640	33×40	2	4	33-20-33
Model 3-D	2700	27×50	2	4	27-40-27
Model 3-E	2640	33×40	2	4	33-40-33

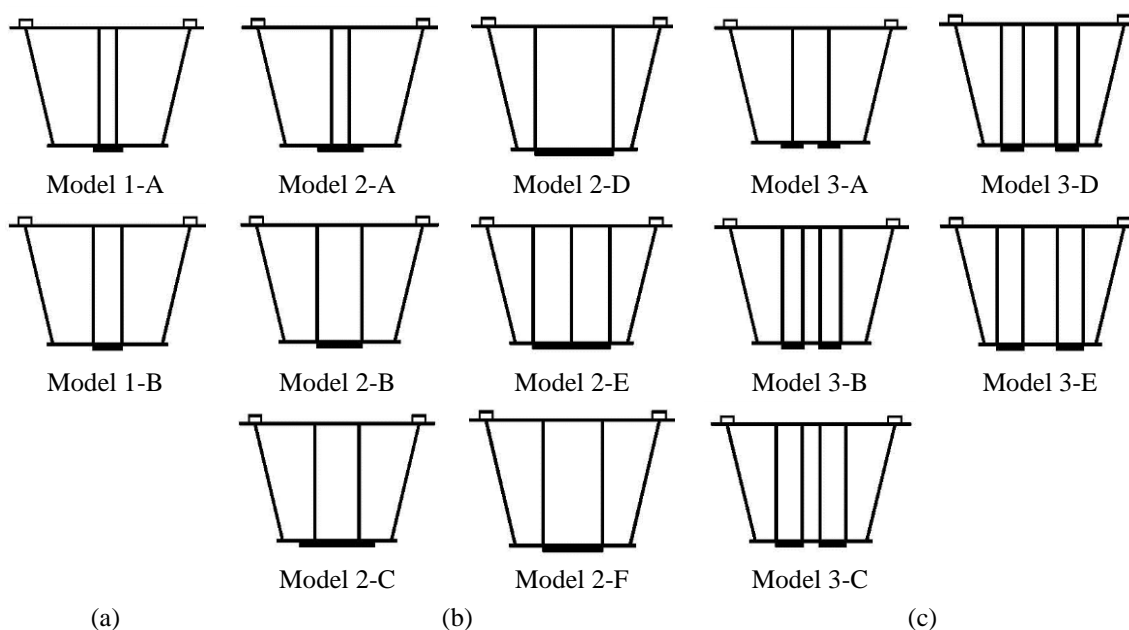


Fig. 3 Different configurations of stiffeners and bearing pads in analytical models (a) Group 1, (b) Group 2 and (c) Group 3

Other than the size of the diaphragm plate, the main parameters that could strongly affect the response of a steel diaphragm are the vertical stiffeners and bearing pads configuration. In order to conduct a useful parametric study, 13 different details of diaphragm configuration are considered

as shown in Fig. 3 and Table 1. Numbers, dimensions and locations of stiffeners and bearing pads have been chosen as variable parameters. Other parameters such as, box girder dimension and diaphragm plate thickness which are related to the overall configuration of the bridge are assumed constant and consistent with the case study model. The scenarios of component changes have been applied as three groups as illustrated in Fig. 3. According to this figure, the first model in group 1 (Model 1-A) is the same as the diaphragm in case study bridge with one bearing pad and 2 pairs of vertical stiffeners. The bearing pad dimension is 900 cm² (30×30cm) and the two pairs of vertical stiffeners are 20 cm apart from each other (see Fig. 1). The stiffeners are moved to 30 cm apart in Model 1-B. The second group (Models 2-A through 2-F) includes a larger single bearing pad area and various vertical stiffener configurations as indicated in Table 1. The third group (Models 3-A through 3-E) consists of two bearing pads and different stiffener configurations. Note that the stiffeners are used in pairs, one on each side of the diaphragm plate and placed symmetrically with respect to the Y axis (Fig. 4).

3. Finite element modeling

In order to have accurate results in nonlinear cyclic dynamic analyses suitable software capable of modeling material and geometric nonlinearities should be chosen. In this study, the ANSYS (2007) general finite element (FE) software is adopted.

It is inefficient and unnecessary to model the whole bridge structure for the study of end diaphragms. Instead, a FE sub-model can more accurately capture the detailed behavior needed without losing accuracy. Therefore, a one meter length of steel box girder containing the target diaphragm with suitable boundary conditions is employed (see Fig. 2). This is similar to FE modeling and test set-up of Megson and Hallak (1995a). Fig. 4 shows the FE model with its components. Rectangular shell elements (Ansysshell-43) with six degrees of freedom and constant thickness are used. Meshing of the elements and boundary condition at its ends are also shown. According to this figure, nodes at the ends of the effective length are restrained in all six degrees of freedom, except for displacements in the transverse and vertical directions (U_x and U_y) which are free to displace as the loads are applied to the flanges. Furthermore, bearing device's nodes at the bottom flange are fixed in three translational degrees of freedom (U_x , U_y and U_z).

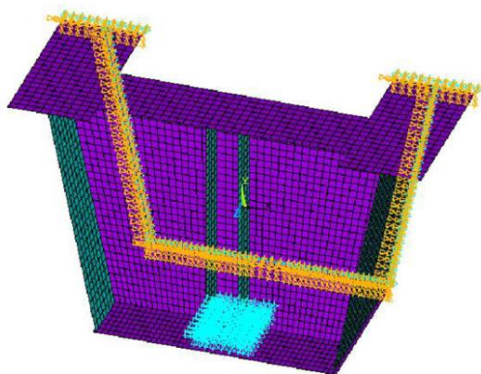


Fig. 4 Model with boundary conditions

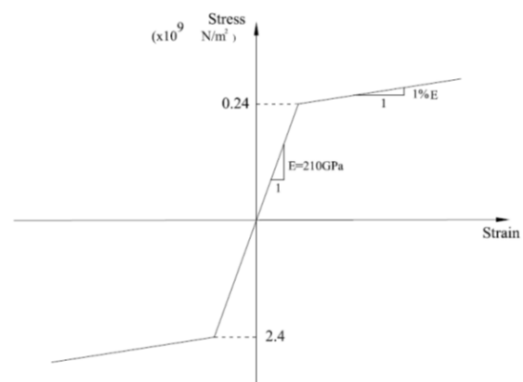


Fig. 5 Steel material behavior

The model is capable of considering the nonlinear behavior of steel material with von Mises yield criterion and plastic flow with kinematic hardening. Steel material used is St-37 with yield strength of 240 MPa, elastic modulus of 210 GPa and an assumed bilinear stress-strain curve according to Fig. 5. The tangent modulus at the onset of strain hardening is taken to be approximately 1% of initial elastic.

4. Applied loads

The models are subjected gradually and in steps to vertical gravity loads first and then the horizontal cyclic seismic displacements are exerted in 20 steps. For the gravity loads, it is very important to apply the loads in the right location to simulate true behavior when using this partial length model. Many loading schemes were tried and stresses were compared to existing test results. Finally, the loading scheme shown in Fig. 6 was adopted. In this scheme, the vertical gravity load is applied as a uniform linear load on top of the two flanges and along the web plate. The calculated results are in agreement with works done by Megson and Hallak (1995b, d). The total vertical load for the case study bridge is the reaction at the support under dead plus live loading and it was found to be equal to 1 MN for each end diaphragm. Furthermore, incremental displacement load representing the lateral cyclic seismic load is applied symmetrically along the length of top two flanges in the vicinity of the top plate width (see Fig. 6). The cyclic lateral displacement loading is shown in Fig. 7. The load includes one cycle of 2,10,20,30, and 40 mm displacements, each one applied in 4 steps. The vertical and lateral load patterns are kept constant throughout the analyses of different models so that the results can be compared.

5. Parametric study

A parametric study is conducted on the 13 different models shown in Fig. 3 with properties as indicated in Table 1. In order to study the diaphragm behavior, vertical and seismic loading conditions are first evaluated separately in the following sections and the influences of effective parameters are determined. Later, the combined loading is discussed.

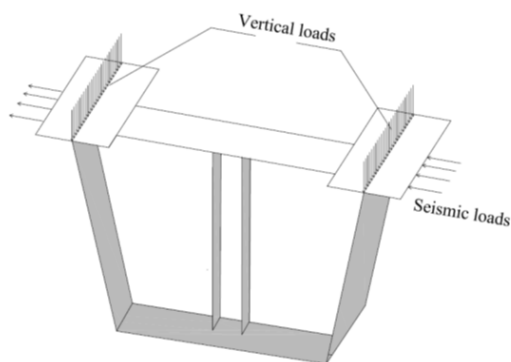


Fig. 6 Vertical and lateral load locations

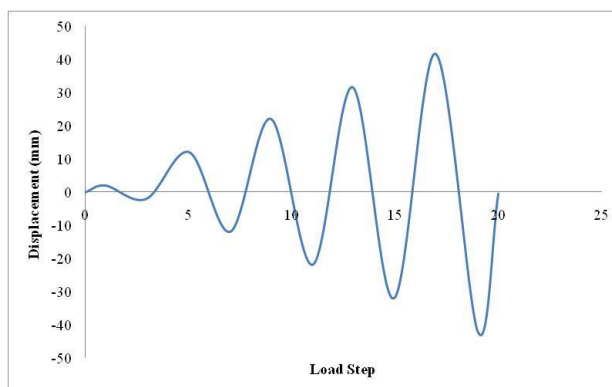


Fig. 7 Seismic cyclic displacement applied in 20 steps

5.1 Effects of vertical load

Stress distributions under the applied vertical load in all diaphragms are evaluated in this section. To better understand the flow of stresses, vertical load is applied incrementally from zero to its maximum value of 1 MN on the two flanges in four steps. Investigating the stress distribution of the diaphragm through the incremental loading provides for better understanding of the effects of diaphragm parameters and flow of forces.

Fig. 8 shows the vertical (S_y), horizontal (S_x) and shear (S_{xy}) stresses in the cross-section of model 1-A under full vertical loading. The stresses are symmetrical with respect to Y axis. The compressive vertical stresses flow from top flanges through the web plates and reach to the bearing pad at the bottom of diaphragm. The diaphragm plate is mainly in compression as expected and maximum stresses occur at the bearing location. For the lower flange and upper plate of the diaphragm horizontal stresses are more important. It is seen that the bottom flange is in compression and the upper plate is in tension. As expected, the shear stresses are very high in the diaphragm plate.

In practice, the combined normal and shearing stresses are needed for the design of diaphragms. The von Mises criterion for yielding under combined stresses is employed by the software. These stresses are always positive and the above introduction was needed to figure out the tension/compression nature of stresses. Fig. 9 shows the von Mises stress distribution under the

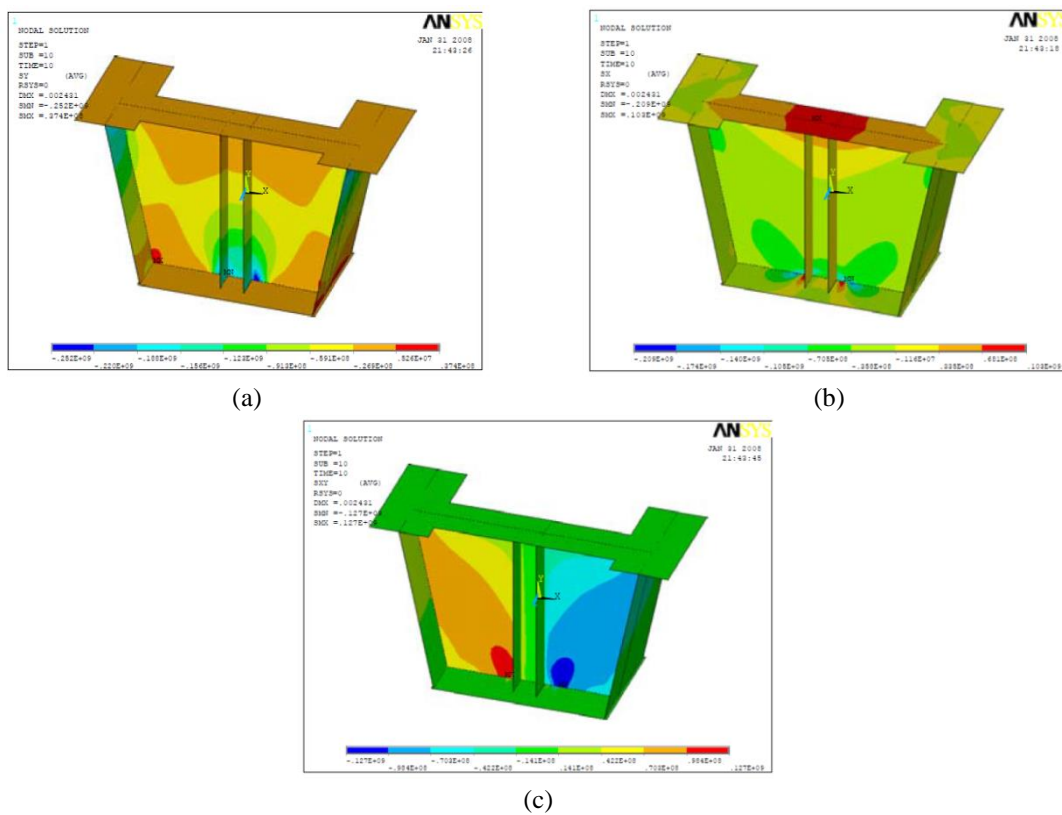


Fig. 8 Stress distribution of model 1-A under vertical loading ;(a) S_y , (b) S_x , (c) S_{xy}

increasing vertical load steps. According to this figure, the stresses in the diaphragm plate at the edges of bearing pad and bottom of stiffeners gradually increase as the load increases. Hence, the maximum stresses are found at the bottom of diaphragm plate just above the bearing device. The increased stresses at the bearing location redistribute through the diaphragm plate diagonally in a butterfly shape. Moreover, tensile stresses occur at the top plate of the diaphragm and grow towards the top flanges as the vertical load increases.

Results of von Mises stresses of all the models at the last step of vertical loading are shown in Fig. 10. The numerical values of von Mises stresses are also tabulated in Table 2. According to the results, the range of maximum stresses in the 13 different models varies from 0.214×10^9 to 0.246×10^9 N/m² at the critical bearing pad location and the bottom of stiffeners.

It can be seen that maximum stresses are almost constant and in the elastic range as designed. Note that, in models 2-B, 2-D, 2-E, 3-B, 3-C, 3-D and 3-E, the distribution of maximum stresses is so limited and also concentrated in the corner of the stiffener that can be neglected. This reduction in stresses is mainly due to the increased number of stiffeners and increased bearing area in these models. The described stress flow from the top flanges to the bottom and its redistribution from the bearing area to the top of the diaphragm obviously show the importance of the diaphragm components. By comparing the models, it is concluded that the maximum stress values are formed at the edge of the bearing pads in all cases. Consequently, it could be implied that increasing the

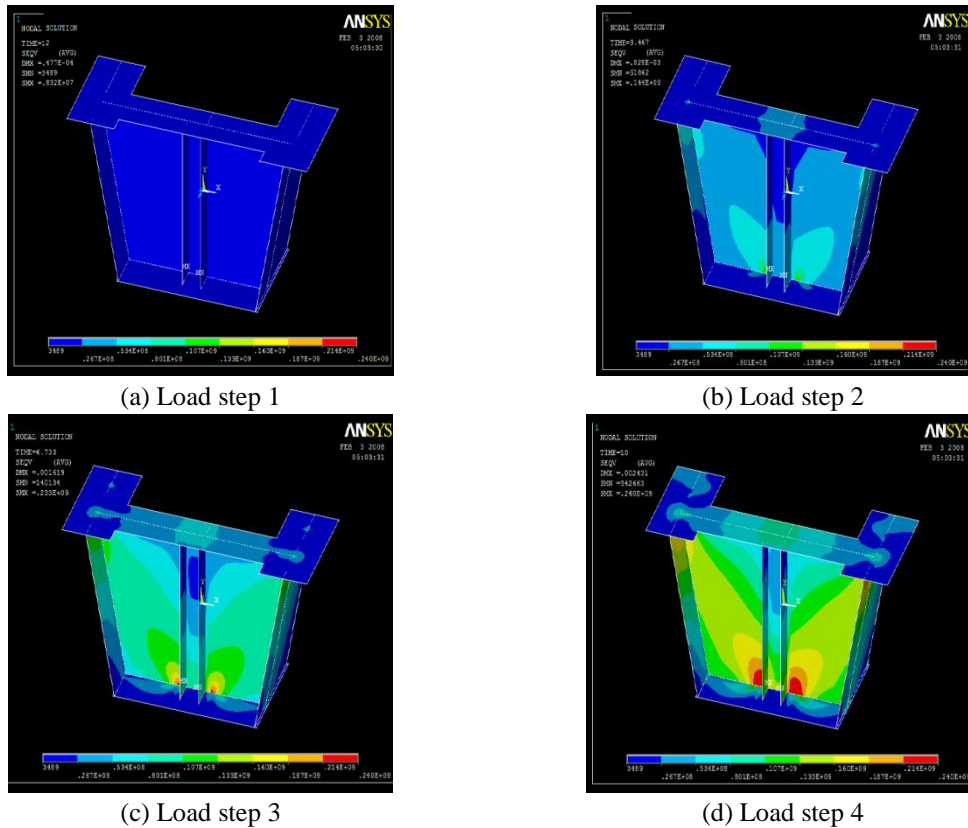


Fig. 9 Stress distribution of model 1-A through different vertical load steps. (a) Load step1, (b)Load step2, (c)Load step 3, (d) Load step 4

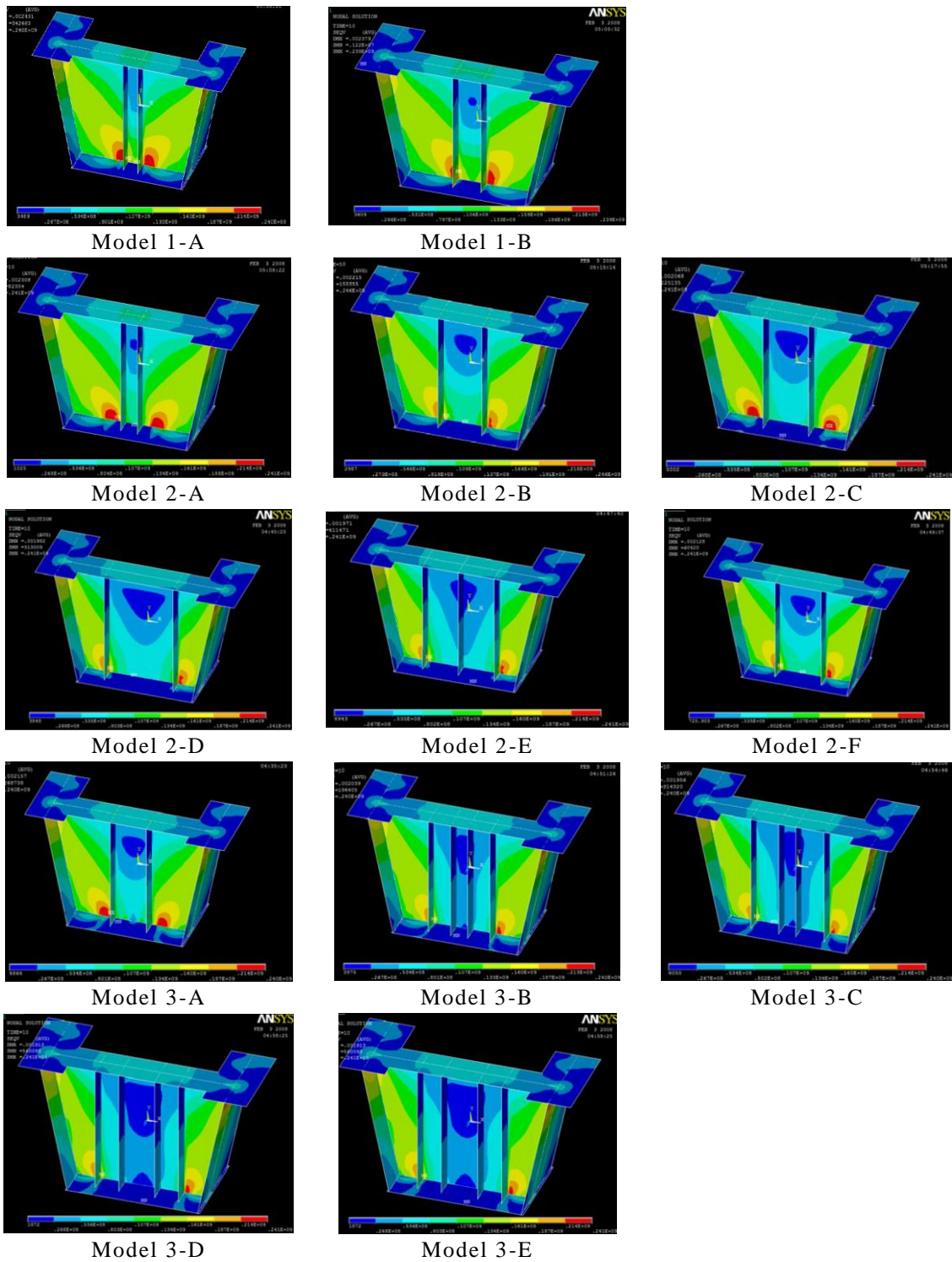


Fig. 10 Stress distribution of different models at the last step of vertical loading

Table 2 von Mises stress variations of different models under full vertical loading

Model	Stress range $\times 10^9 \text{ N/m}^2$	Description
Model 1-A	0.240–0.214	
Model 1-B	0.239–0.213	
Model 2-A	0.240–0.214	
Model 2-B	0.246–0.218	<i>The domain of the 0.246 is so limited which could be neglected</i>
Model 2-C	0.241–0.214	
Model 2-D	0.241–0.214	<i>The domain of the 0.241 is so limited which could be neglected</i>
Model 2-E	0.241–0.214	<i>The domain of the 0.241 is so limited which could be neglected</i>
Model 2-F	0.241–0.214	
Model 3-A	0.241–0.214	
Model 3-B	0.241–0.214	<i>The domain of the 0.241 is so limited which could be neglected</i>
Model 3-C	0.241–0.214	<i>The domain of the 0.241 is so limited which could be neglected</i>
Model 3-D	0.241–0.214	<i>The domain of the 0.241 is so limited which could be neglected</i>
Model 3-E	0.241–0.214	<i>The domain of the 0.241 is so limited which could be neglected</i>

area of the bearing pads and locating the stiffeners at the location of maximum stresses (edge of bearing pads) would be helpful in reducing the stresses. Increasing the number of vertical stiffeners also reduces stresses in the diaphragm plate and the maximum tensile stresses at the top plate of the diaphragm.

5.2 Seismic lateral load effects

5.2.1 End diaphragm components interaction

The response of the end diaphragm system under lateral loading is more complicated due to the contribution of different components. In other words, the existence of the other elements such as external diaphragm, deck and their connections makes the stress distribution different so that different response could be achieved by altering them. An extra research has been developed on the complete end diaphragm models in order to evaluate the components contribution. Due to the main purpose of the paper which is evaluating the different configuration of internal box girder diaphragm, a brief summary of its contribution as part of the end diaphragm for lateral supporting system is provided. Fig. 11 shows different components at the end diaphragm for lateral resistant.

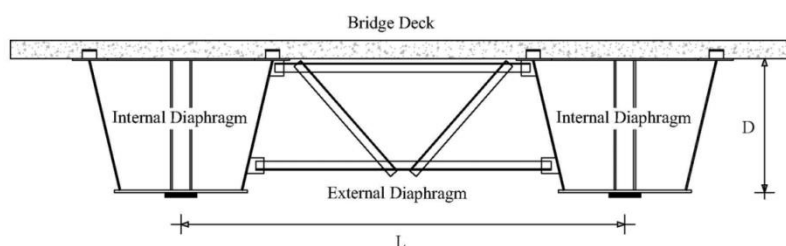


Fig. 11 Different components of model No.1 with its end diaphragm

The study shows that some important parameters would affect the diaphragm response significantly under lateral seismic loading. The parameters include; 1) Type and configuration of external diaphragm, 2) End diaphragm aspect ratio (L/D), 3) Bearing device used below the box girder, 6) thickness of the slab with rigid or flexible action and 7) Internal diaphragm configuration. Some of the parameters were also investigated in other researches (Helwig *et al.* 2007, Helwig and Yura 2012). The detailed evaluation of each item is ignored due to length limitation of the manuscript and just internal diaphragm is investigated here. This study shows that internal diaphragm could be significantly affecting the response under lateral loads; however the participation of the internal diaphragm is strongly affected by its interaction with other elements. Due to the special boundary conditions of this element, its performance is similar to the Steel Plate Shear Wall (SPSW) with significant absorbed energy and stable hysteretic loops. The way stress is distributed and the location of local yielding and buckling govern its behavior. Consequently, configuration of the stiffeners could strongly affect the behavior. The remaining part of the paper investigates the internal diaphragm behavior with different stiffener and support configurations.

5.2.2 End diaphragm under lateral load

Stress distribution under lateral cyclic load is the key parameter in understanding the diaphragm components behavior in an earthquake. As mentioned before, a review of literature shows that the cyclic behavior of diaphragms has not been studied previously. Therefore, model 1-A is first subjected to lateral cyclic loading (as in Fig. 7) for a detailed study. The results at final stage of lateral loading are shown in Fig. 12. As can be seen, the vertical stress in the diaphragm plate is just as high as the horizontal stress in the bottom flange. They occur at the stiffeners location and are symmetrical. The von Mises strains (not shown) for Model 1-A is about 0.03 at the same location. This indicates that steel has yielded but undamaged in this area. The shear stresses are high in the region between the two vertical stiffeners. However, its numerical value is in the order of one half of normal stresses.

Detailed review of the stresses show that the bottom flange governing stress is the horizontal S_x stresses with positive and negative signs for each half length of the plate. The top plate acts similarly with much lower stresses. Note that, in composite bridges the slab on top acts as a horizontal rigid diaphragm and the top plate would have no stresses in it. However, our model here has no concrete on top. The diaphragm plate is mainly governed by the vertical S_y stresses except for the space between the stiffeners where shear stresses S_{xy} are also high.

In order to see the combined stresses, the von Mises stresses at the initial and final steps of loading for selected models are shown in Fig. 13. As seen, the critical stress distribution starts from the bottom of diaphragm plate and at the edges of the bearing pads. The combined stresses are symmetric with respect to the vertical Y axis and as noted previously, have opposite signs. As the load increases, the stresses distribute radially upward in the diaphragm plate with maximum values still at the base. Eventually, the high stresses reach the stiffeners and the top plate. The steel material stays in its elastic range at the first cycles of loading and there would be no significant residual stress after unloading. Later, as the applied cyclic displacements increase, the material enters into the nonlinear range and consequently residual stresses and strains would remain in the diaphragm at unloading steps. The complete hysteretic behavior of the Group 2 diaphragms under the cyclic displacements is shown in Fig. 14. It is seen that the behavior is stable with excellent energy absorbing feature (area under the curves). In fact, this was expected as well. Such stiffened diaphragms perform like Steel Plate Shear Walls (SPSW) which is becoming increasingly popular in seismic design of buildings. Comparing the Group 2 cases, one can conclude that wider stiffener

spacing and bearings have beneficial effects against seismic loads. Model 2-C carried slightly over 2 MN of lateral load.

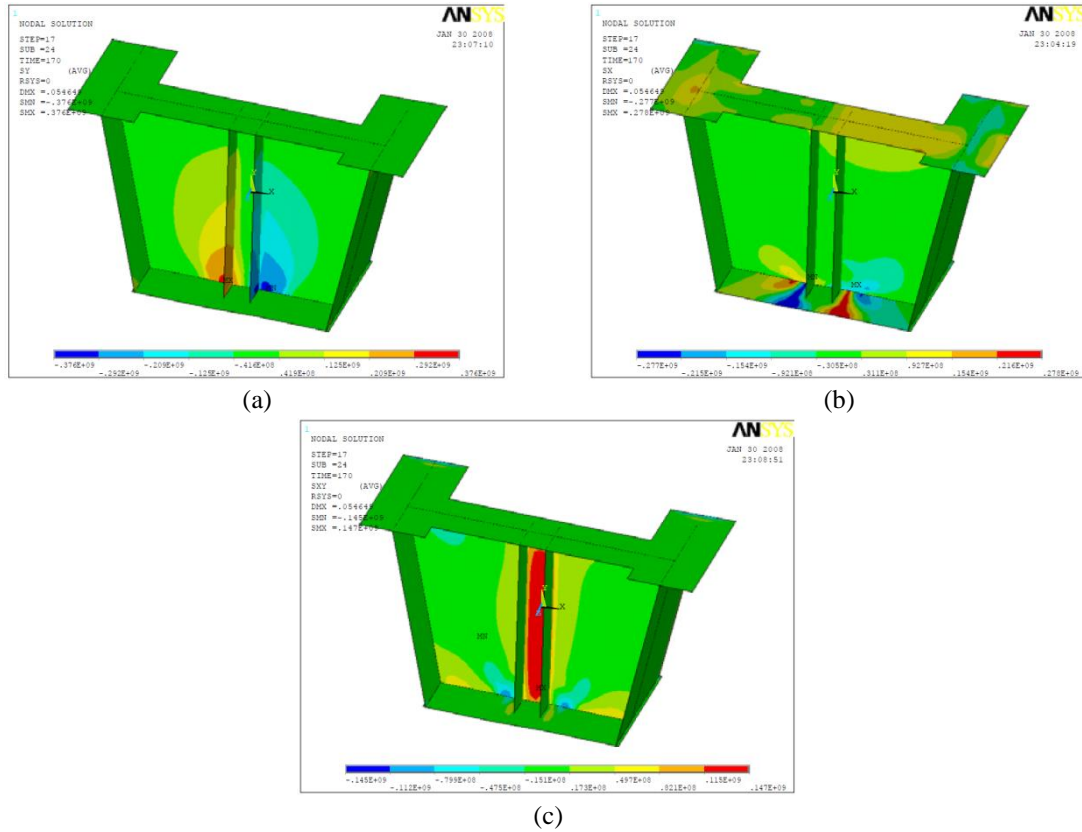


Fig. 12 Stress distribution of model 1-A under lateral cyclic loading only, load step 17; (a) vertical S_y stresses, (b) horizontal S_x stresses, (c) shear S_{xy} stresses

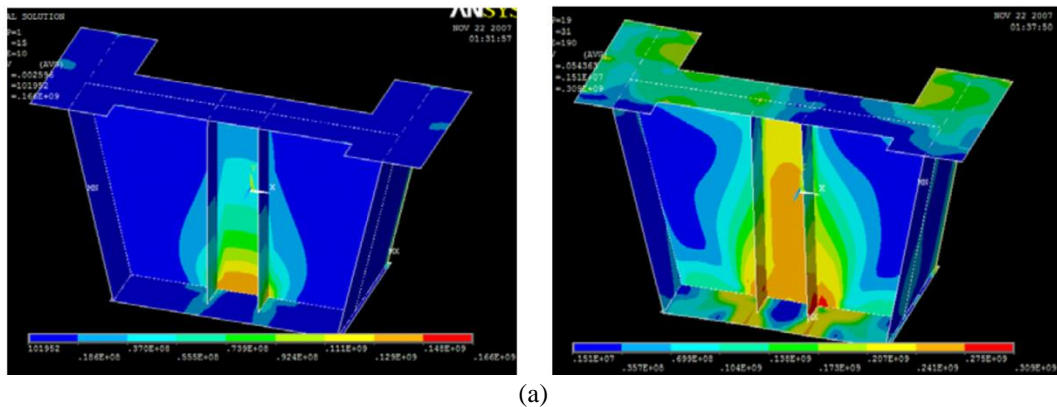


Fig. 13 von Mises stress distribution of models under lateral cyclic loading (left=initial, right=final); (a)1-A, (b) 2-E, (c) 3-E

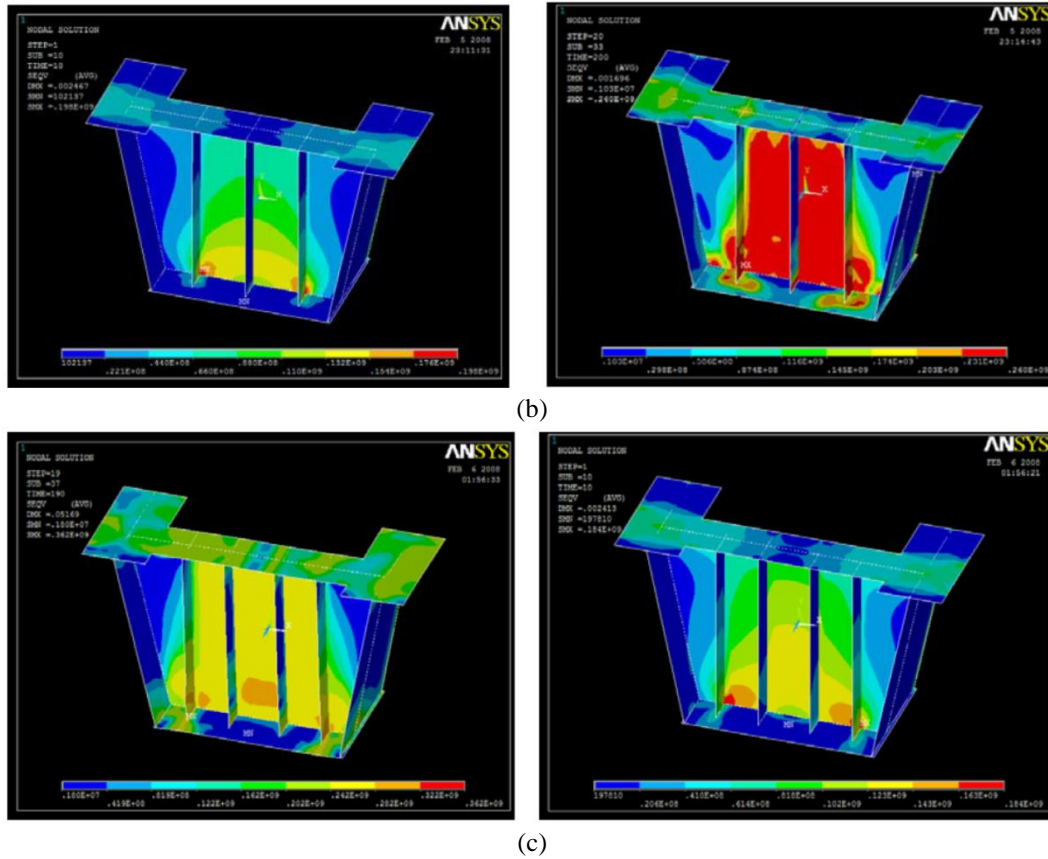


Fig. 13 Continued

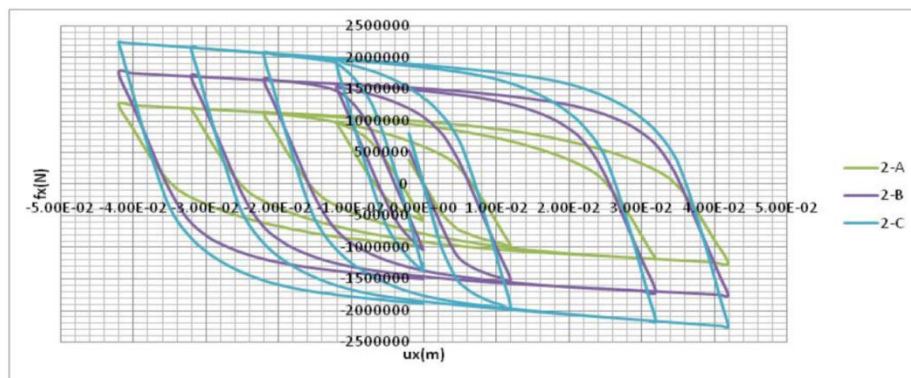


Fig. 14 Hysteresis behavior of models 2A, 2B and 2C

5.2.3 End diaphragm under combined load

Given the fact that in reality vertical loads on diaphragms are always present when an earthquake happens, evaluation of the diaphragm behavior under combined vertical and cyclic seismic loads is considered next. Therefore, the models are first loaded with the vertical loading as

above and then the cyclic lateral displacement load (see Fig. 7) is applied incrementally. The results for von Mises stresses at the final step of loading are shown in Fig. 14 for selected models.

The numerical values of maximum von Mises stresses in different parts of the diaphragm are shown in Table 3. Under the vertical load steps, as noted before, diagonal distribution of stresses in the diaphragm plate initiates. As the lateral load increases, the combined von Mises stress distribution changes to a more uniform pattern throughout the diaphragm. The maximum stress is still at the bottom of the diaphragm and at the edge of the stiffeners. From Table 3 it is seen that the edge of the stiffener, the diaphragm plate and the bottom flange all carry about the same amount of stress.

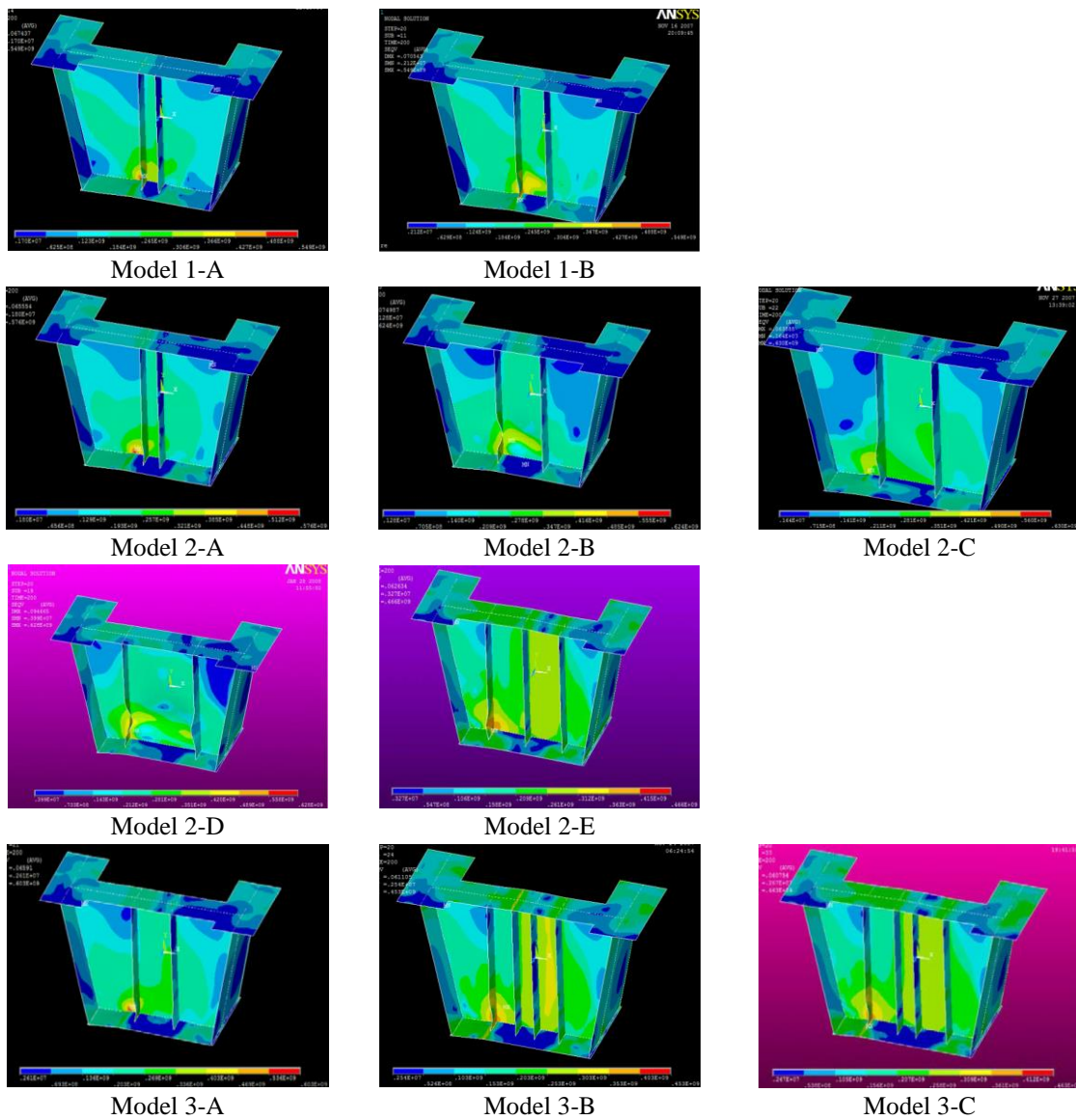
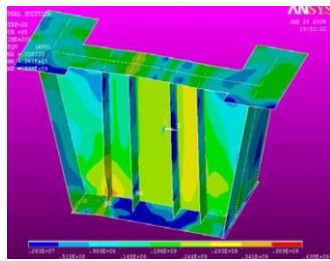
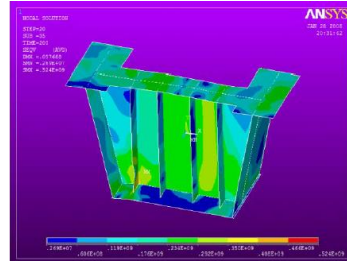


Fig. 15 von Mises stresses under combined vertical and seismic loads, final step



Model 3-D



Model 3-E

Fig. 15 Continued

Table 3 Maximum von Mises stresses in different components of diaphragms at final load step

Model	Maximum Stresses						Absorbed Energy ×10 ⁵ N.m
	Top Flange	Top Plate	Web	Stiffeners	Diaphragm Plate	Bottom Flange	
	×10 ⁹ N/m ²						
1-A	0.2442	0.2145	0.2752	0.4091	0.5110	0.5110	1.07
1-B	0.2455	0.2402	0.2787	0.4489	0.5554	0.4555	1.43
2-A	0.2454	0.2411	0.2827	0.3699	0.5416	0.5416	1.53
2-B	0.2444	0.2504	0.2863	0.4799	0.4334	0.4798	2.40
2-C	0.2443	0.2589	0.2774	0.3570	0.5940	0.5940	3.24
2-D	0.2442	0.2427	0.2953	0.5423	0.4717	0.5452	3.78
2-E	0.2472	0.2788	0.2781	0.4348	0.4345	0.4348	4.33
2-F	0.2443	0.2512	0.2930	0.5244	0.4379	0.5244	3.05
3-A	0.2444	0.2447	0.2929	0.4494	0.5759	0.5759	2.66
3-B	0.2442	0.2805	0.2856	0.4376	0.4007	0.4376	3.59
3-C	0.2442	0.2756	0.2890	0.4332	0.3985	0.4321	4.28
3-D	0.2443	0.2774	0.2856	0.4280	0.3897	0.4280	4.67
3-E	0.2465	0.2806	0.2885	0.4501	0.4026	0.4500	5.31

Note that, any stress above 0.24×10^9 N/m² indicates yielded material. The maximum stress is 0.594×10^9 N/m² which corresponds to a strain of 0.18 mm/mm. This is assumed as the onset of failure for ST-37 steel here. In order to understand the seismic response of diaphragms and the amount of energy absorption under such loads, the hysteretic curves of different models under seismic loading are presented in Fig. 15. The absorbed energy due to hysteretic behavior, which is defined as the inner area of hysteretic loops, is also provided in Table 3.

Comparing the results shows that changing the diaphragm configuration can affect both the maximum stresses and/or the total absorbed energy. For example, Table 3 illustrates that increasing the bearing pad area from 30×30 cm (model 1-A) to 50×50 cm (model 2-A) does not change the maximum stresses in the diaphragm components significantly. However, the absorbed energy in cyclic loading increases about 1.43 times (see Fig. 16). This shows that bearing area has beneficial effects in seismic loading.

Comparing the values of model 1-A and 1-B shows that increasing the distance of stiffeners

increases the stresses at top plate, stiffeners and diaphragm plate, but the stress at the bottom flange decreases. Moreover, the configuration improves the absorbed hysteretic energy about 1.34 times. Increasing the distance between stiffeners from 20 cm (model 2-A) to 50 cm (model 2-B) causes 30% increase in stiffener stresses but the absorbed energy increases by 57%. Meanwhile, the diaphragm plate stress is reduced by 20%. This shows that wider stiffener spacing distributes the stresses in the diaphragm more uniformly. In addition, by increasing both the bearing pad area and stiffener distance, the absorbed energy is raised about 2.24 times (compare models 1-A and 2-B).

The changes made in model 2-C illustrate the effects of bearing pad's dimensions. Comparing the results of models 2-B and 2-C, it is seen that by keeping constant the area of the bearing pad and by increasing the length of the bearing pad along the web plate, the maximum stresses which are located in the bottom of diaphragm increase and stresses in the stiffeners are reduced. In this case, the absorbed energy is improved by 35% with respect to model 2-B.

Similar to model 1-B, comparing the results of model 2-C, 2-D and 2-F shows that increasing the distance of stiffeners causes an increase in the stresses of the web plate and stiffeners, but the stresses at bottom flange and diaphragm are decreased significantly by locating the stiffeners at the edge of the bearing pad. The absorbed hysteretic energy increases about 17% in model 2-D

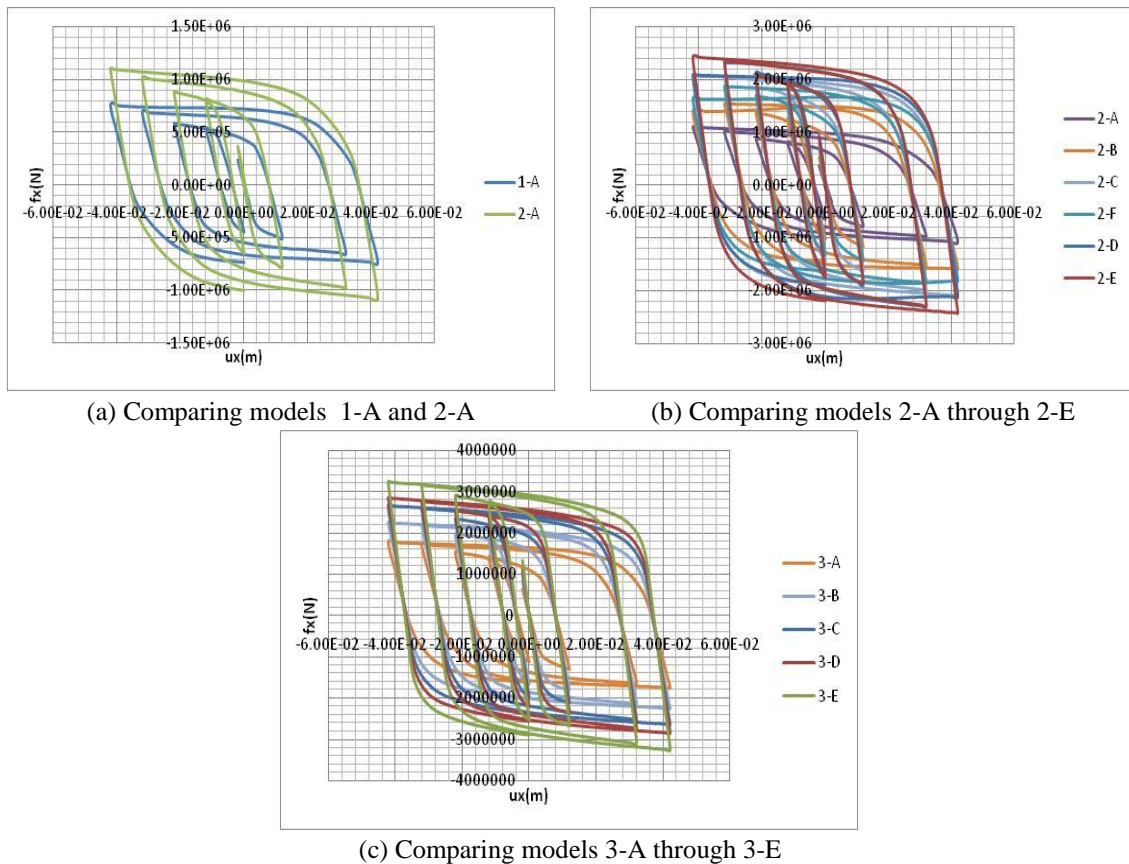


Fig. 16 Hysteretic curves of different models under seismic loading

compared to model 2-C. Moreover, further increase in the distance between stiffeners in model 2-F decreases the absorbed energy by 6%. The situation could be further improved as in model 2-E by adding an extra stiffener at center of the diaphragm and moving the outer stiffeners to the bearing pad edges. In this model, the stresses in all components of diaphragm (except top plate) are reduced significantly and consequently the absorbed energy is increased by 34% and 283% with respect to models 2-C and 2-A, respectively.

Furthermore, numbers of bearing pads and stiffeners are evaluated in group 3 models. By keeping constant the area of the bearing pads, number of them is increased in this group. Model 3-A has two bearing pads with two stiffeners in which each stiffener is located at the center of the pad. This change improves the results for absorbed energy as compared to model 1-A by 248%. It is also much more than models 2-A and 2-B. Therefore, using two bearing pads significantly improves the seismic performance. By using two additional stiffeners located at the edges of the bearing pads as in model 3-B, the results are further improved from model 3-A. The absorbed energy is increased by 35% and the amount of maximum stresses is reduced.

Next, the dimensions of bearing pads are increased along the diaphragm as in model 3-C. In this model, the distance of the inner stiffeners is not changed and is about 20 cm. The results show that the changes increase the stresses slightly and also the absorbed energy reaches to 1.19 and 1.61 times of models 3-B and 3-A, respectively. Maintaining the configurations of models 3-B and 3-C, the distance of the inner stiffeners is increased to 40 cm in model 3-D and 3-E. This increase helps by decreasing the maximum stresses in different components of the diaphragm and consequently the absorbed energy is increased from 24 to 30%. The increase is also about from 75% to 100% with respect to model 3-A.

In summary, comparing the different models with different diaphragm configurations shows that a key parameter in order to improve the seismic behavior is locating the stiffeners at the edge of the bearing pads. In this case, the stresses are transferred effectively to the stiffeners and the maximum stresses at the bottom of diaphragm are decreased. Also it improves the stress distribution and increases the absorbed hysteretic energy. Another parameter that could affect the results significantly is the distance between stiffeners. By increasing this distance, stresses are decreased in most of the components. Moreover, area and number of the bearing pads are important components, such that the area increase reduces maximum stresses and increases the absorbed energy. Furthermore, increasing l/w ratio (ratio of length to width) of bearing pads results an extension of the bearing length along the diaphragm and helps by reducing stresses and improving the amount of absorbed energy. Also, adding an extra stiffener to the center of the web plate is another important change which could improve the responses.

Among the 13 different models that were studied here, model 3-D has the best seismic response such that maximum stresses and strains of this model are significantly lower than the other models. Moreover, in this case the absorbed hysteretic energy is much higher than the other models and its value is about 4.36 times of the base model 1-A.

6. Conclusions

In this study, using a nonlinear 3D finite element model, the performance of stiffened steel diaphragms of tub girder bridges under vertical and cyclic seismic loads were evaluated. A partial model with shell elements that includes the vertical stiffeners and bearing pads with appropriate boundary conditions was introduced. The location of application of vertical reaction and seismic

load was determined to simulate true behavior. Furthermore, different scenarios of diaphragm configurations were considered by using 13 different models altering number and area of bearing pads, number and location of stiffeners and bearing pad's l/w ratio. Influence of the diaphragm components was evaluated step by step for each loading. Consequently, the most efficient diaphragm configuration for combined vertical and seismic loads was introduced.

Based on the analyses performed the following suggestions for the design of stiffened diaphragms at the end of steel tub girders can be given:

- Under vertical loading, the stresses flow through the web plates and bottom flange and into the bearing pads. The maximum stresses in diaphragm plates are formed at the base of the diaphragm near the bearings and as they move diagonally like butterfly wings on each side of the stiffeners the magnitude of these stresses are reduced. These stresses are mainly shear S_{xy} stresses. Moreover, there is a considerable tensile S_x stress in the bottom flange of the girder.

- Under pure lateral cyclic loading, the maximum stresses are formed at the location of the bearing pads and they distribute symmetrically in the diaphragm plate with maximum values in the space between stiffeners. These stresses are mainly vertical S_y stresses.

- Under combined vertical and lateral loading, the location of maximum stresses is at the bottom of diaphragm near bearings. The stresses distribute uniformly throughout the diaphragm plate from bottom to top.

- The maximum stresses are decreased as the bearing pad area is increased and it causes a better stress distribution through the web plate and consequently the absorbed energy is increased.

- The maximum stresses at the edges of bearing pads are decreased as the distance between stiffeners is increased. By placing the stiffeners at the maximum stress locations, the stresses in the stiffeners increases and are decreased in the web plate. Consequently, the stiffeners stresses are increased slightly, but stress distribution and absorbed energy are improved.

- Increasing the number of bearing pads and stiffeners improve the results by better stress distribution and decreasing the maximum stress values and also increasing the absorbed energy.

- Increasing the l/w ratio (ratio of length to width) of bearing pads could be helpful in seismic response and improves the stress distribution and absorbed energy.

- Adding extra stiffeners to the center of the diaphragm improves the stress distribution at the web plate, decreases the maximum stresses and strains of the other stiffeners and also increases the absorbed energy.

- Among the 13 different models that were studied here, model 3-D has the best seismic response such that maximum stresses and strains of this model are significantly lower than the other models.

References

- AASHTO (2002), *Standard specifications for highway bridges*, American Association of State Highway and Transportation Officials, 17th ed., Washington D.C.
- ANSYS (2007), *Structural Analysis Guide*, ANSYS Inc.
- Choi, Y.C. and Oh, B.H. (2013), "Transverse modeling of concrete box-girder bridges for prediction of deck slab ultimate load capacity", *J. Bridge Eng.*, **18**(12), 1373-1382.
- Chusilp, P., Usami, T., Ge1, H., Maeno, H. and Aoki, T. (2002), "Cyclic shear behavior of steel box girders: experiment and analysis", *Earthq. Eng. Struct. Dyn.*, **31**(11), 1993-2014.
- Crisfield, M.A. and Puthli, R.S. (1977), "A finite element method applied to the collapse of stiffened box girder diaphragms", *International Symposium of Steel Plated Structures*, London.

- Dean, J.A. (1975), "The collapse behavior of steel plating subject to complex loading", Ph.D. Dissertation, University of London.
- Dean, J.A. and Dowling, V.J. (1973), "Steel box girders, stiffened load bearing diaphragms: Construction, instrumentation and initial imperfection measurements and analysis of test results", Engineering Structures Laboratories, Civil Engineering Department, Imperial College, London. CESLIC Reports BGS 24 and 30.
- Einarsson, B., Crisfield, M.A. and Dowling, P.J. (1982), "Collapse of stiffened box-girder diaphragms" *J. Constr. Steel Res.*, **2**(2), 11-25.
- Helwig, T., Yura, J., Herman, R., Williamson, E. and Li, D. (2007), "Design guidelines for steel trapezoidal box girder systems", Center for Transportation Research, Report No. 0-4307-1, University of Texas, Austin.
- Helwig, T. and Yura, J. (2012), "Steel bridge design handbook; Bracing system design", U.S. Department of Transportation, Report No. FHWA-IF-12-052, Washington, D.C.
- Herman, R.S., Li, D. and Helwig, T.A. (2005), "Trapezoidal box girder bridge bracing: Results from field monitoring and FEA", Proceedings: *ASCE Structures Congress*.
- Irwin, C.A.G. and Loe, J.A. (1978), "Loading tests on the stiffened diaphragms of a trapezoidal steel box girder", Transport and Road Research Laboratory, Report LR824, Crowthorne, Berks.
- Kargarmoakhar, R., Chowdhury, A.G. and Irwin, P. (2015), "Reynolds number effects on twin box girder long span bridge aerodynamics", *Wind Struct.*, **20**(2), 327-347.
- Kaveh, A., Bakhshpoori, T. and Barkhori, M. (2014), "Optimum design of multi-span composite box girder bridges using Cuckoo Search algorithm", *Steel Compos. Struct.*, **17**(5), 705-719.
- Kim, K. and Yoo, C.H. (2006), "Brace forces in steel box girders with single diagonal lateral bracing systems", *J. Struct. Eng.*, **132**(8), 1212-1222.
- Kim, K. and Yoo, C.H. (2009), "Bending behaviors of quasi-closed trapezoidal box girders with X-type internal cross-frames", *J. Constr. Steel Res.*, **65**(8-9), 1827-1835.
- Kim, J. and Williamson, E.B. (2014), "Finite-element modeling of twin steel box-girder bridges for redundancy evaluation", *J. Bridge Eng.*, **20**(10), 04014106.
- Megson, T.H.G. and Hallak, G. (1995a), "Finite element modeling of box girder diaphragms at supports", *Thin-Wall. Struct.*, **22**(1), 25-37.
- Megson, T.H.G. and Hallak, G. (1995b), "Optimum design of box girder having supports at the flange/web junctions", *Thin-Wall. Struct.*, **22**(1), 39-49.
- Megson, T.H.G. and Hallak, G. (1995c), "Optimum design of load-bearing box girder diaphragms having a central support", *Thin-Wall. Struct.*, **22**(3), 203-215.
- Megson, T.H.G. and Hallak, G. (1995d), "Optimum design of load-bearing box girder diaphragms having supports at a distance from the flange/web junctions", *Thin-Wall. Struct.*, **22**(4), 275-289.
- Memberg, M.A., Yura, J.A., Williamson, E.B. and Frank, K.H. (2002), "A design procedure for intermediate external diaphragms on curved steel trapezoidal box girder bridges", FHWA/TX-03/1898-1 Report.
- Nie, J.G. and Zhu, L. (2014), "Beam-Truss model of steel-concrete composite box-girder bridges", *J. Bridge Eng.*, **19**(7), 04014023.
- Park, N.H., Choi, Y.J. and Kang, Y.J. (2005), "Spacing of intermediate diaphragms in horizontally curved steel box girder bridges", *Finite Elem. Anal. Des.*, **41**(9-10), 925-943.
- Samaras, V.A., Sutton, J.P., Williamson, E.B. and Frank, K.H. (2012), "Simplified method for evaluating the redundancy of twin steel box-girder bridges", *J. Bridge Eng.*, **17**(3), 470-480.
- Schexnayder, C., Alarcon, F.A., Antillo, E.D., Morales, B.C. and Lopez, M. (2011), "Observation on bridge performance during the Chilean earthquake of 2010", *J. Constr. Eng. Manage.*, ASCE, **140**(4), B4013001.
- Yen, P.W., Chen, G.D., Buckle, I., Allen, T., Alzamora, D., Ger, J. and Arias, J.G. (2014), "Bridge performance during the 2010 M8.8 Chile Earthquake", *ASCE Structures Congress*.
- Zsarnóczyay, A., Vigh, L.G. and Kollár, L.P. (2014), "Seismic performance of conventional girder bridges immoderate seismic regions", *J. Bridge Eng.*, **19**(5), 04014001.